Chapter V

Adsorption Studies using TTIH

The discussion pertaining to the experimental observations of trapping the selected metal ion using treated ***Tamarindus indica*** **Hull** (TTIH) is dealt in this chapter.

5.1 Microscopic, BET and BJH Analyses

The microscopic image of TTIH is illustrated in figure 5.1. Particle size distribution and mesoporous nature of TTIH, being evident from BET and BJH plots (Figures 5.2 - 5.4) reveal the surface area and mean pore diameter to be 0.325 m^2/g and 52.33 nm respectively (Table 5.1). The pore diameter lying in between 20 Å and 500 Å, refer to the predominance of mesopores.

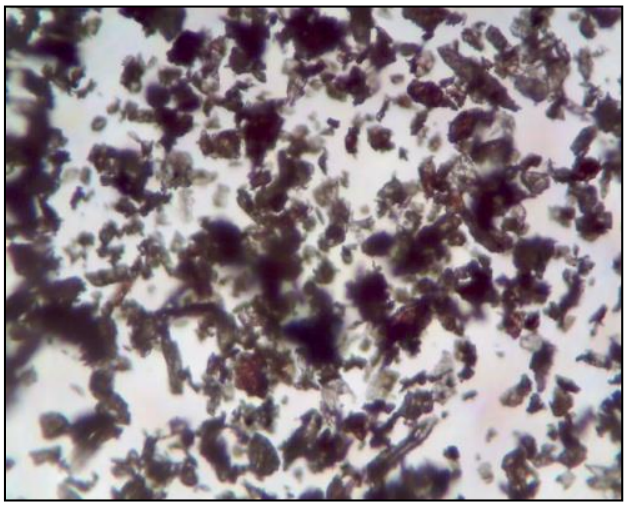

Figure 5.1 Microscopic View

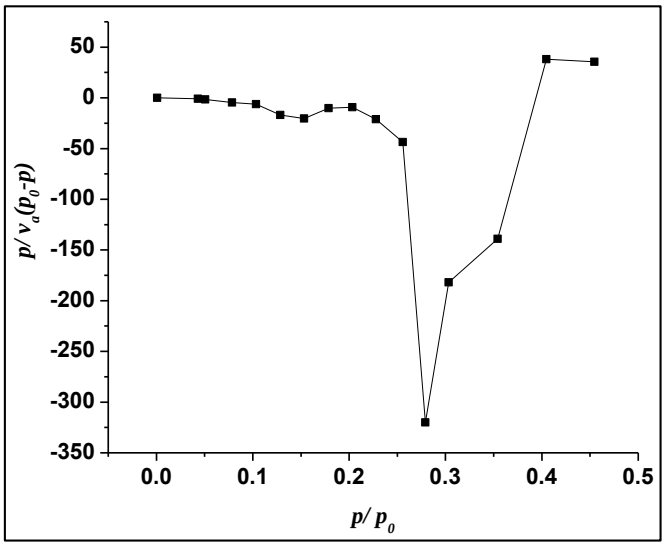

Figure 5.2 BET Plot

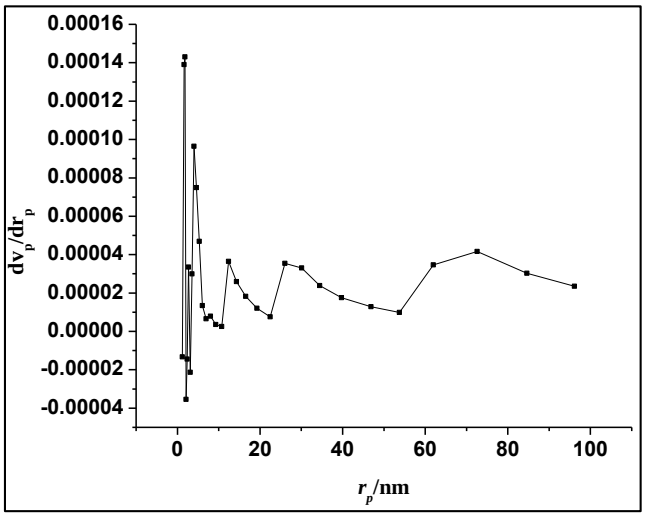

Figure 5.3 BJH Plot

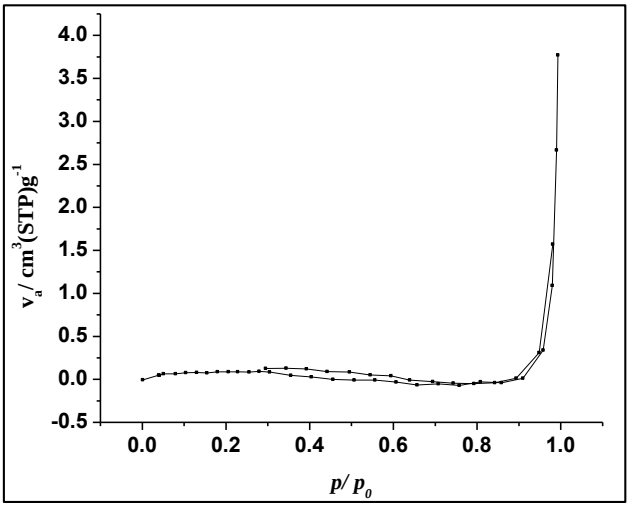

Figure 5.4 Adsorption/ Desorption Plot

5.2 TTIH - Characterization

The characteristics properties viz., bulk density, specific gravity, moisture and ash content exhibit lower values for TTIH similar to that of TPJB, as evident from table 5.1. Acid/ water soluble matter values are observed to be lower, favouring the insoluble nature of TTIH, thereby aiding its use in the acidic/ basic environments. pH_{ZPC} value of TTIH also favours the sorption of cations onto the former's surface. Against other studied elements/ groups, more carbon content and carboxylic groups of TTIH promote the sorption capacity due to electrostatic interaction property[116].

Table 5.1 Physiochemical Characterization

Properties	TTIH
pH (1 % solution)	6.15
Conductivity	35.50
Moisture (%)	1.54
Bulk density (g/L)	0.55
Specific gravity	1.47
Porosity	62.59
Ash content (%)	3.29
Water soluble matter (%)	2.89
Acid soluble matter (%)	1.68
Ion exchange capacity (meq/g)	0.41
pH_{zpc}	5.9
Surface area (m^2/g)	0.325
Mean Pore diameter (nm)	52.33
Carbon (%)	44.08
Nitrogen (%)	0.92
Hydrogen (%)	5.35
Sulphur (%)	Nil
Surface Acidic Groups (mmol/g)	
Phenolic	0.32
Carboxylic	1.12
Lactonic	0.15

5.3 SEM and EDAX Analyses

Figure 5.6 registered a high porous nature, rough texture of base TTIH as compared with that of its raw material (Figure 5.5), whereas figures 5.7 - 5.9, exhibit defined morphologies corresponding to the binding of Pb(II), Cd(II) and Ni(II) ions onto the TTIH surface.

EDAX spectra of unloaded TTIH and metal laden counterparts are presented in figures 5.10 - 5.13. Appearances of new peaks at 2 to 8 keV in loaded figures confirm the chelation of respective ions by the treated material.

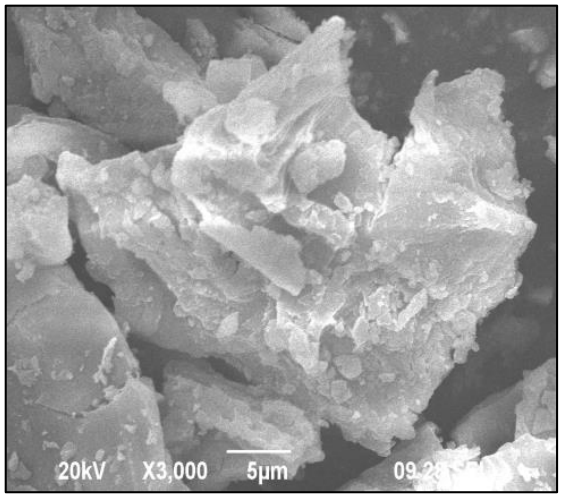

Figure 5.5 SEM: TIH

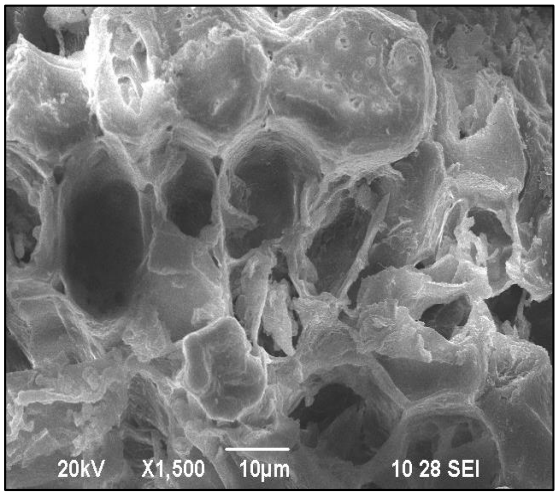

Figure 5.6 SEM: TTIH

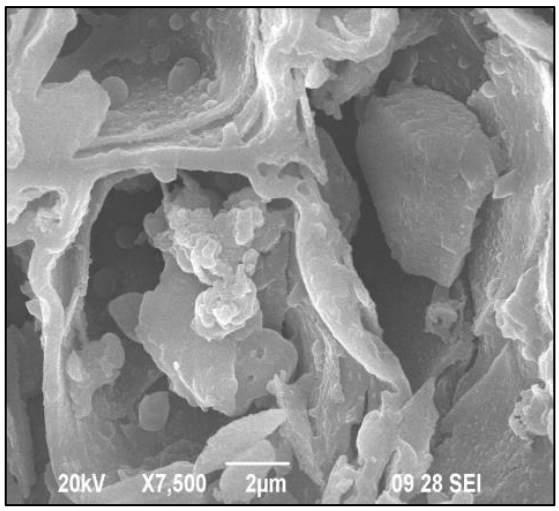

Figure 5.7 SEM: Pb(II) - TTIH

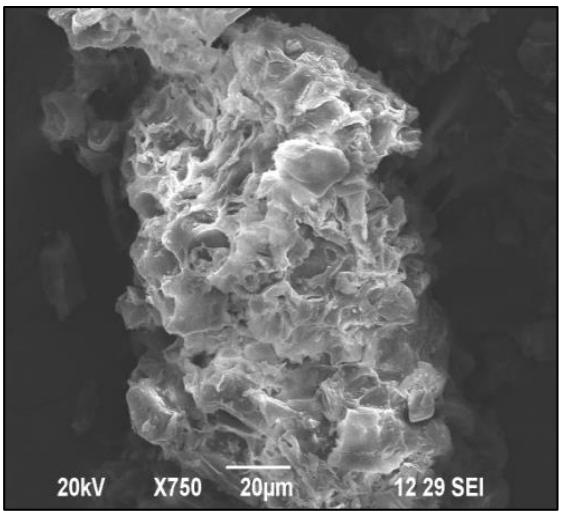

Figure 5.8 SEM: Cd(II) - TTIH

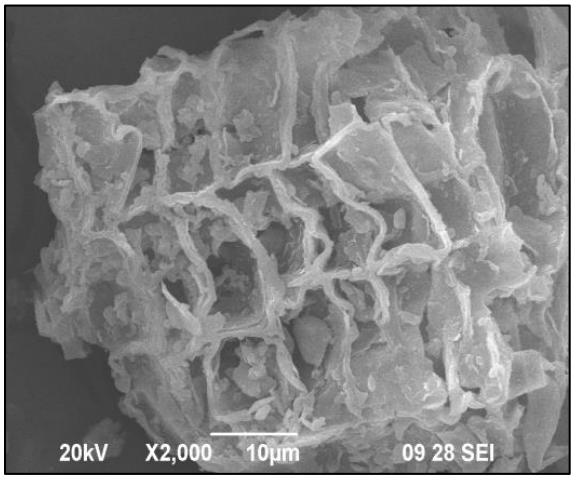

Figure 5.9 SEM: Ni(II) - TTIH

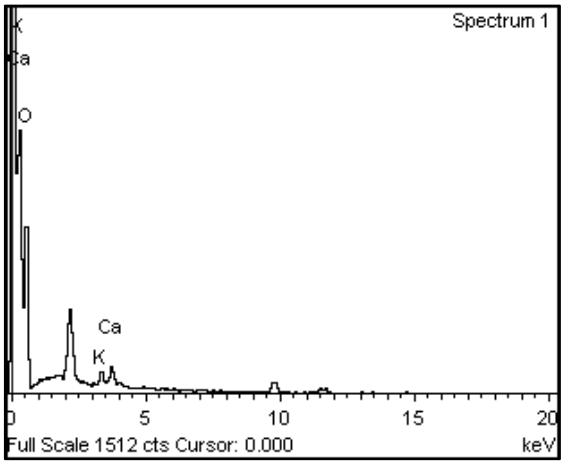

Figure 5.10 EDAX: TTIH

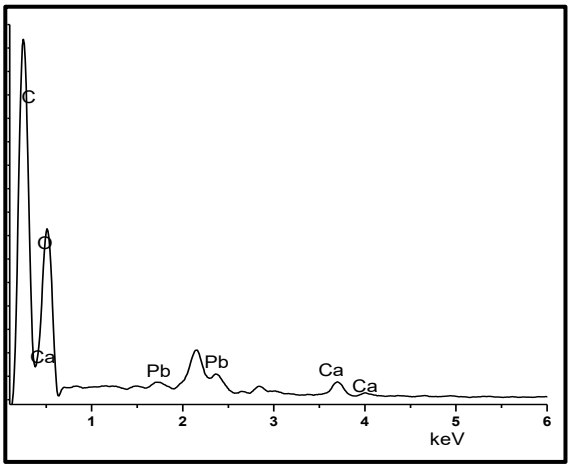

Figure 5.11 EDAX: Pb(II) - TTIH

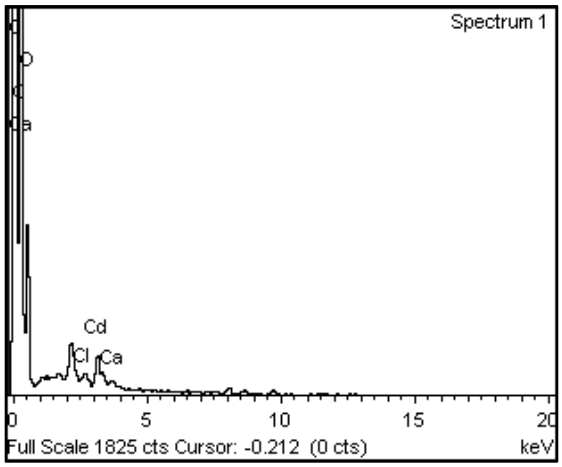

Figure 5.12 EDAX: Cd(II) – TTIH

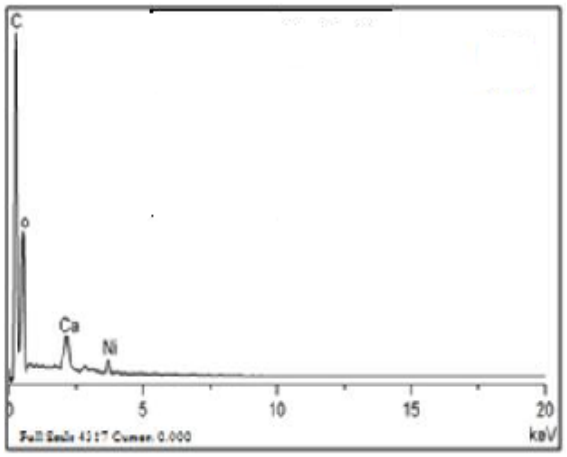

Figure 5.13 EDAX: Ni(II) - TTIH

5.4 FTIR Spectral Studies

FT-IR spectra of unloaded TTIH [Figure 5.14(a)] has several distinct peaks at 3632.12 cm^{-1}, 2317.57 cm^{-1}, 1729.26 cm^{-1}, 1455.35 cm^{-1} and 1019.42 cm^{-1}, assigned to –OH (hydroxyl group), H-C-H, –C=O (lactones, quinine and carboxylic acids)[97], C-H (methylene group) and –C-O stretching[102] correspondingly. The spectra of Pb(II) loaded TTIH [Figure 5.14(b)] exhibits peak shifts corresponding to the functional groups viz., 3765.21 cm^{-1} (-OH), 2313.71 cm^{-1} (H-C-H), 1734.08 cm^{-1} (C=O), 1505.51 cm^{-1} (C-H) and 1037.75 cm^{-1} (C-O). The variations observed in peak intensities and positions favour the involvement of surface functional groups in the process of Pb(II) sorption.

Similar shift of C=O (1603.88 cm^{-1}), C-O (1032.93 cm^{-1}) and obvious disappearance of -OH, H-C-H, C=O peaks in figure 5.14(c), represent the deprotonation and the feasible formation of cadmium oxygen bond formation during sorption. Figure 5.14(d) depicts the intensity and peak variations [3581 cm^{-1} (-OH), 2313.71 cm^{-1} (H-C-H), 1741.80 cm^{-1} (C=O), 1511.29 cm^{-1} (C-H) and 1036.78 cm^{-1} (C-O)] pertaining to Ni(II) removal against the base TTIH.

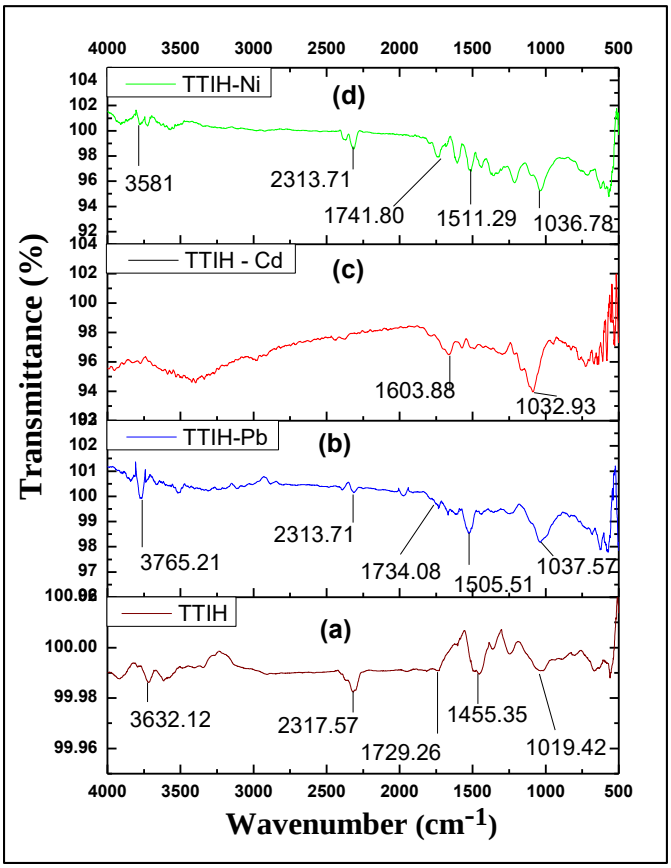

Figure 5.14 FTIR Spectra

5.5 Batch Equilibration Experiments

5.5.1 Effect of Particle Size

A trend of sorption reduction is observed at increased particle sizes[154, 155] (0.18 mm – 0.71 mm) as evident from table 5.2. Maximum adsorption capacity is evident for 0.18 mm (shown as bold values) for the chosen metal ions and thence 0.18 mm is optimized for the following studies.

Table 5.2 Effect of Particle Size

Metal Ions	Amount Adsorbed (mg/g)				
	0.18 mm	**0.24 mm**	**0.30 mm**	**0.42 mm**	**0.71 mm**
Pb(II)	**13.20**	11.73	9.78	10.27	9.94
Cd(II)	**12.55**	11.41	10.76	9.94	8.80
Ni(II)	**8.68**	8.07	7.21	6.35	5.86

5.5.2 Effect of Initial Concentration and Agitation Time

Metal uptake with more or less identical representations [Figures 5.15 - 5.17] is single, smooth, continuous curves towards saturation[153]. Maximum amounts of **13.40, 12.82** and **12.41 mg/g** being adsorbed for an initial concentration of 100 mg/L at a contact time of 20 minutes for Pb(II), Cd(II) and 30 minutes for Ni(II) respectively, followed by declines is evident.

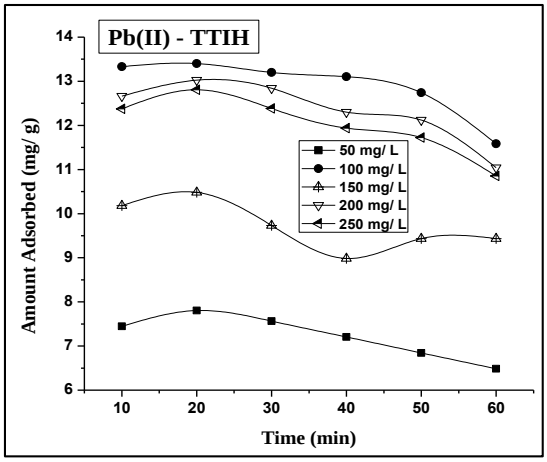

Figure 5.15 Effect of Initial Concentration and Agitation Time- Pb(II)

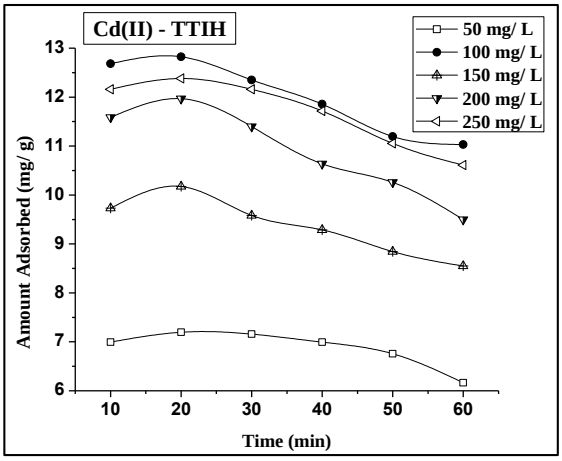

Figure 5.16 Effect of Initial Concentration and Agitation Time- Cd(II)

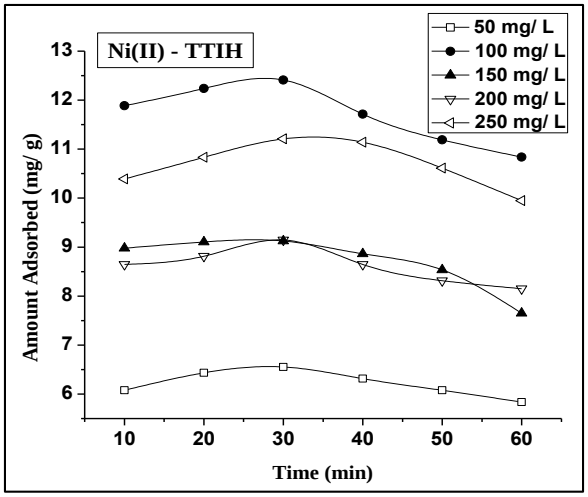

Figure 5.17 Effect of Initial Concentration and Agitation Time- Ni(II)

5.5.3 Effect of Dosage

The influence of TTIH dosages (100 – 500 mg: 100 mg) at varying time slots are shown in figure 5.18. The cumulative rise in the q_e values of dosage reflects on the increase in the surface area available for adsorption due to the enhancement of active sites, facilitating, favourable penetration of metal ions[156]. Maximum adsorption had occurred at dose of 300 mg for Pb(II), Cd(II) and 400 mg for Ni(IasmaI) correspondingly at predetermined time intervals. Further decline in sorption rate [157, 126, 158], implicit the active sites' saturation on TTIH surface.

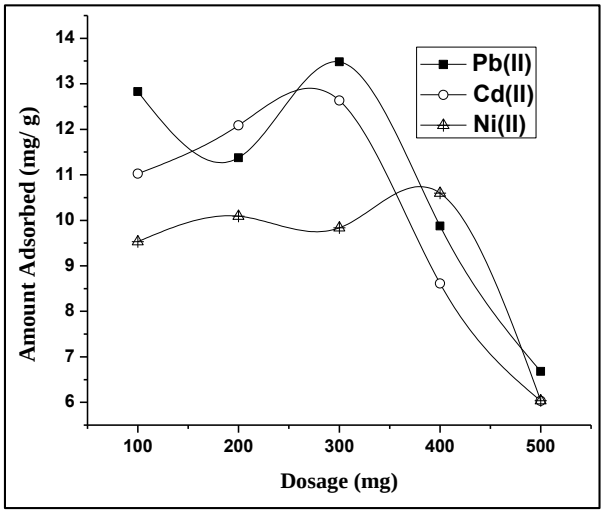

Figure 5.18 Effect of Adsorbent Dose

5.5.4 Effect of pH

pH profiles of Pb(II), Cd(II) and Ni(II) removal by TTIH is shown in figure 5.19, where occurrence of maximum sorption is noticed at pH 5 for Pb(II)/ Ni(II) and pH 7 for Cd(II) - ions. A decline in sorption rate may be emphasized due to insoluble metal hydroxide precipitation at alkaline pH ranges[138].

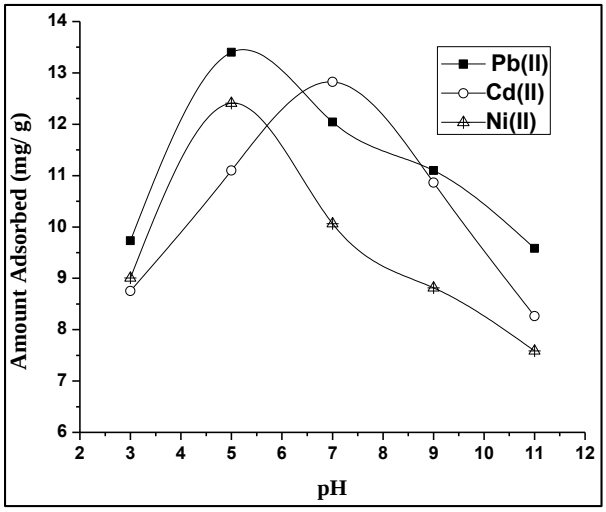

Figure 5.19 Effect of pH

5.5.5 Effect of Cations/ Anions/ Co-ions

An extended apparent inhibition in metal ion removal is evident from table 5.3 in presence of K^+ ions, rather than Mg^{2+} ions[131]. Similar to previous experimental discussions 4.6.5, an extensive impact of Cl^- ions on metal ion sequestration[155] using TTIH is evident. Co-ionic results also indicate that divalent Zn and hexavalent Cr show marked inhibition in metal ion trapping.

Table 5.3 Effect of Cations, Anions and Co-ions

Metal Ions	Percentage Removal (%)						
	Absence of Ions	Cations		Anions		Co-ions	
		K^+	Mg^{2+}	Cl^-	SO_4^{2-}	Zn^{2+}	Cr^{6+}
Pb(II)	81.68	76.43	79.43	74.22	75.63	76.88	74.43
Cd(II)	77.82	73.37	74.87	72.36	73.92	71.24	72.05
Ni(II)	71.24	62.05	62.76	60.04	61.83	63.61	65.38

5.5.6 Effect of Temperature

The effect of temperature (293-333 K: 10 K) as illustrated in table 5.4, reveal that the adsorption percentage has raised from 78.92 to 83.68 %, 71.08 to 81.84% and 69.27 to 73.12% for Pb(II), Cd(II) and Ni(II) ions, correspondingly. The enhancement in the percentage removal against temperature may relate to the increase in mobility of ions or the active diffusion sites, which may make small pores to wider and provide more surfaces for sorption[159, 160]. Since, maximum removal had occurred at 303 K, it is fixed as optimum temperature for the studies.

Table 5.4 Effect of Temperature

Temperature (K)	Percentage Removal (%)		
	Pb(II)	Cd(II)	Ni(II)
293	78.92	71.08	69.27
303	81.01	77.82	71.28
313	82.54	78.38	72.43
323	83.07	79.45	73.12
333	83.68	81.84	72.92

5.5.7 Desorption and Regeneration Studies

Figure 5.20 shows a trend of maximum desorption at 0.02 M HCl (eluent), indicative of inverted parabola. The results of desorption experiments imply a maximum of 79.52, 74.63, 73.45% using regenerated TTIH for Pb(II), Cd(II), Ni(II) respectively. Regeneration cycles calculated for successive adsorption are expressed as bar diagrams [Figure 5.21], which shows a similarity in the process.

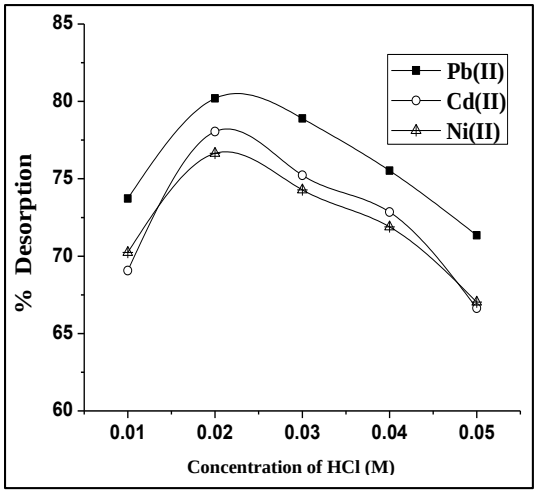

Figure 5.20 Desorption – TTIH

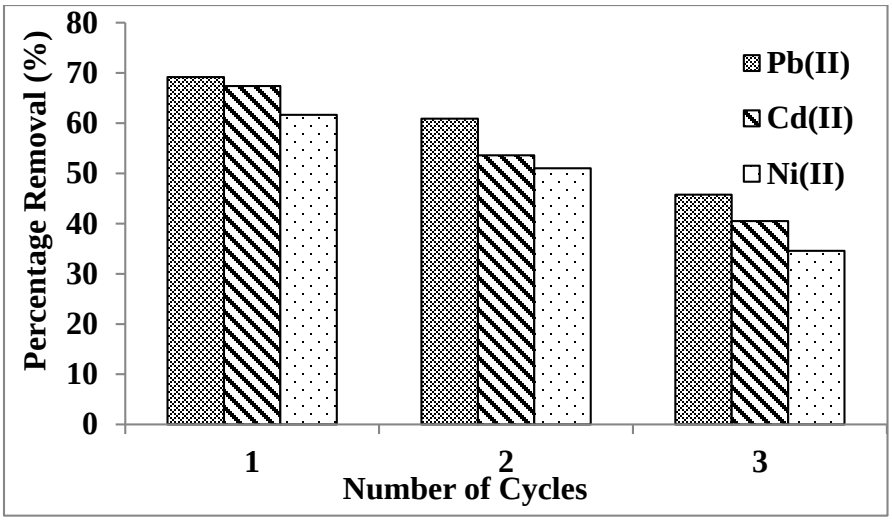

Figure 5.21 Regeneration - TTIH

5.6 Adsorption Isotherms

The obtained data pertaining to the batch experiments are applied to the Langmuir, Freundlich, Tempkin and Dubinin- Radushkevich isotherm models, in order to verify the best linear fit for Pb(II), Cd(II) and Ni(II) – TTIH systems and calculated axes values are shown in table 5.5. The isothermal constants derived from respective plots are listed in table 5.6.

Table 5.5 Equilibrium Concentrations

Conc. of Metal Ions (mg/L)	Langmuir		Freundlich		Tempkin		DKR	
	C_e	C_e/q_e	log C_e	log q_e	ln C_e	q_e	ε^2 X10^{-5}	ln q_e
Pb(II)								
50	16.81	2.15	1.22	0.89	2.82	7.80	0.21	2.05
100	18.86	1.40	1.27	1.12	2.93	13.40	0.16	2.59
150	44.92	4.28	1.65	1.02	3.80	10.48	0.03	2.34
200	50.65	3.88	1.70	1.11	3.92	13.02	0.02	2.56
250	88.99	6.94	1.94	1.10	4.48	12.80	0.07	2.55

Conc. of Metal Ions (mg/L)	Langmuir		Freundlich		Tempkin		DKR	
	C_e	C_e/q_e	log C_e	log q_e	ln C_e	q_e	ε^2 X10^{-5}	ln q_e
Cd(II)								
50	18.63	2.58	1.27	0.85	2.92	7.19	0.17	1.97
100	21.85	1.70	1.33	1.10	3.08	12.82	0.12	2.55
150	45.70	4.49	1.65	1.00	3.82	10.17	0.02	2.31
200	70.28	5.87	1.84	1.07	4.25	11.96	0.01	2.48
250	97.27	7.85	1.98	1.09	4.57	12.38	0.06	2.51
Ni(II)								
50	21.44	3.27	1.33	0.81	3.06	6.55	0.13	1.87
100	30.41	2.45	1.48	1.09	3.41	12.41	0.06	2.51
150	55.91	6.12	1.74	0.96	4.02	9.12	0.02	2.21
200	74.83	8.18	1.87	0.97	4.31	9.14	0.01	2.21
250	108.98	9.72	2.03	1.04	4.69	11.20	0.05	2.41

Table 5.6 Isothermal Constants

Isotherm Parameters	Pb(II)	Cd(II)	Ni(II)
Langmuir			
q_m (mg/g)	14.10	12.87	12.34
b (L/g)	0.09	0.05	0.06
R^2	0.9971	0.9922	0.9937
Freundlich			
K_F (mg/g)	3.38	2.79	2.31
n	3.34	2.99	3.02
R^2	0.9853	0.9756	0.9504

Isotherm Parameters	Pb(II)	Cd(II)	Ni(II)
Tempkin			
A_T (L/g)	1.17	0.79	0.71
b_T	17.03	12.90	7.47
R^2	0.8966	0.8589	0.8859
DKR			
q_s (mg/g)	13.15	12.52	12.02
E (kJ/mol)	4.57	4.14	3.66
R^2	0.8648	0.8614	0.7942

5.6.1 Langmuir Isotherm Model

The fit in of the Langmuir isotherm (C_e/q_e vs C_e) as depicted in figure 5.22 implies the linearity of the plotted values. The monolayer adsorption capacities (q_m) as indicated in table 5.6 are 14.10, 12.87 and 12.34 mg/g for Pb(II), Cd(II) and Ni(II) respectively, which are found to be better than oil palm shell[161], coconut husk[162], sugarcane bagasse[163] in the sorption Pb(II): 3.39 mg/g; Cd(II): 8.58 mg/g and Ni(II): 2 mg/g. The above fact is supported by free energy of sorption 'b' and R^2 values. The R_L values calculated from Langmuir constant 'b' and initial concentrations of respective metal ions in the process of adsorption using TTIH is listed in table 5.7. The range of these values between 0 and 1 i.e; 0.03 and 0.28 refer to favorability of the adsorption system.

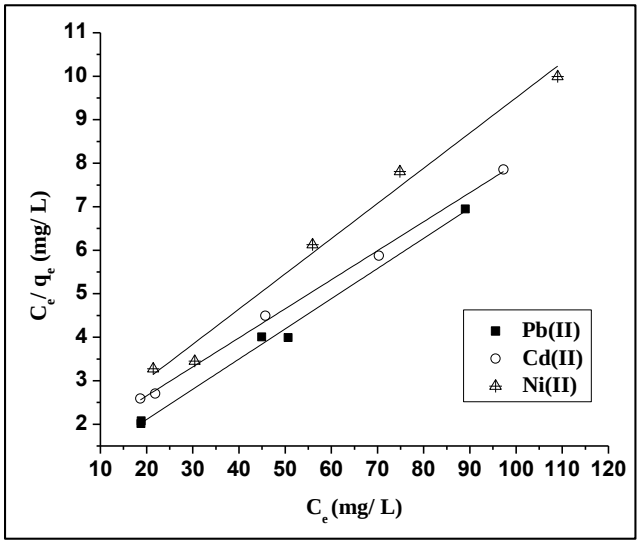

Figure 5.22 Langmuir Isotherm Model

Table 5.7 Equilibrium Parameter R_L

Conc.(mg/L)	Pb(II)	Cd(II)	Ni(II)
50	0.17	0.28	0.25
100	0.09	0.16	0.14
150	0.06	0.11	0.10
200	0.04	0.08	0.07
250	0.03	0.07	0.06

5.6.2 Freundlich Isotherm Model

K_F and 1/n generated from the intercepts and slopes of the Freundlich plot (Figure 5.23) correspond to the sorption capacity and sorption intensity of TTIH in the removal of Pb(II), Cd(II) and Ni(II). A significant variation between the q_e values (at an optimum concentration) and K_F values imply slight deviations of log q_e and log C_e points, favouring better linearity in case of Langmuir isotherm.

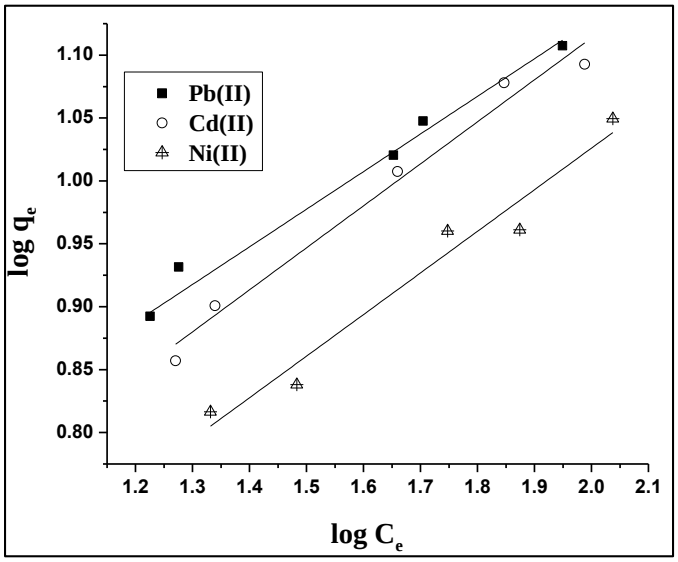

Figure 5.23 Freundlich Isotherm Model

5.6.3 Tempkin Isotherm Model

Tempkin constants A_T and b_T are obtained from the linear plot of q_e vs ln C_e (Figure 5.24) These constants, along with the correlation co-efficient values are lower than Pb(II), Cd(II) and Ni(II) – TPJB systems, denoting non-applicability of the model against Langmuir and Freundlich models[72].

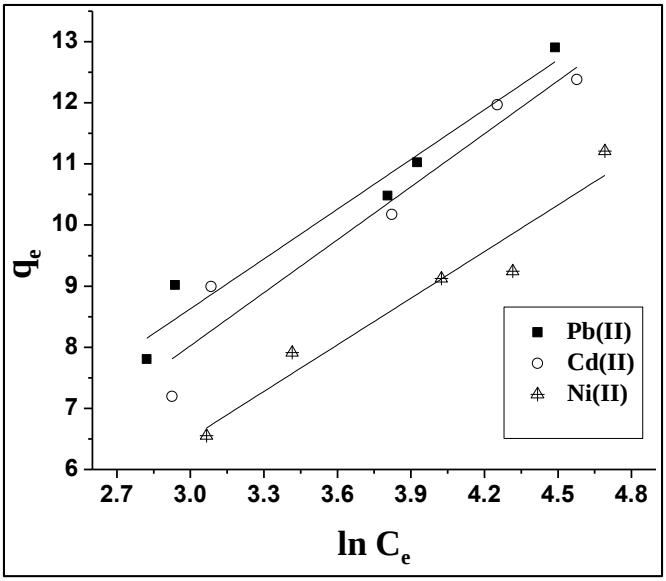

Figure 5.24 Tempkin Isotherm Model

5.6.4 Dubinin– Kaganer -Radushkevich Isotherm Model

The DKR plots (ln q_e vs ε^2) for the adsorption of Pb(II), Cd(II) and Ni(II) are shown in figure 5.25 from whose slopes the mean sorption energy are calculated, being 4.57, 4.14 and 3.66 kJ/ mol. However, chemisorption is mode of adsorption when these values are greater than 8 kJ/ mol. Since, the current values are lower than above specified value, support physisorption mode, confirming the best suitability of Langmuir equation to the studied systems, wherein monolayer adsorption is most favoured[123,164].

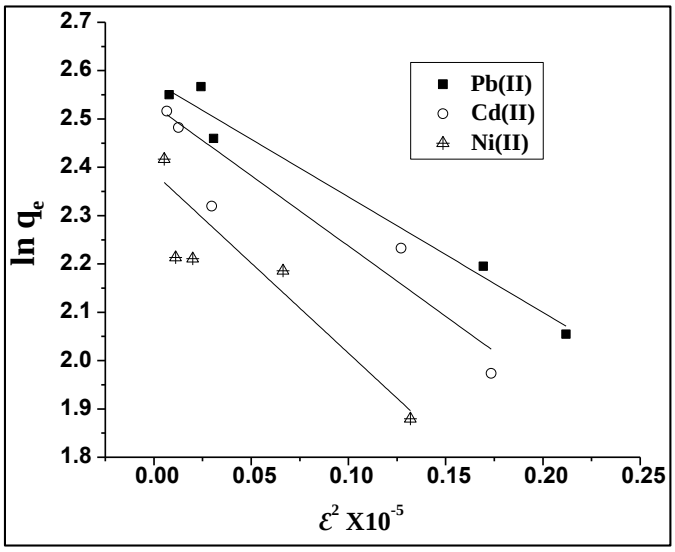

Figure 5.25 Dubinin-Kaganer-Radushkevich Isotherm Model

5.7 Adsorption Kinetics

Various kinetic models viz., pseudo-first-order, pseudo-second-order, Elovich and Intraparticle diffusion models are discussed as done in previous chapter.

5.7.1 Pseudo-First-Order/ Pseudo-First-Order Models

The y-axes values for pseudo-first-order and pseudo-second-order plots (Figures 5.26 and 5.27) were derived from the adsorption capacities observed at specific time intervals (q_t) for the three metal ions and are shown in table 5.8. The rate constants K_1, K_2 and q_{cal} values obtained from their respective plots along with q_{exp}, R^2 values are mentioned in table 5.9. Sum of squares of errors as given by the difference between q_{exp} and q_{cal} is observed to be minimal for the pseudo-second-order kinetics than its counter parts, thereby concluding the better agreement of the systems with this model. Similar reports are available in literature for metal removal using cyanobacterium biomass[137].

Table 5.8 Pseudo-First-Order / Pseudo-Second-Order Kinetics

Time (min)	Pb(II)			Cd(II)			Ni(II)		
	q_t	$\log (q_e-q_t)$	t/q_t	q_t	$\log (q_e-q_t)$	t/q_t	q_t	$\log (q_e-q_t)$	t/q_t
10	13.32	4.44	0.75	12.68	1.93	0.77	12.88	1.93	0.84
20	13.47	4.44	1.49	12.82	1.93	1.55	12.23	1.93	1.63
30	13.19	4.44	2.27	12.34	1.93	2.42	12.41	1.93	2.41
40	13.10	4.45	3.05	11.85	1.93	3.37	11.71	1.93	3.41
50	12.73	4.45	3.92	11.19	1.94	4.46	11.18	1.94	4.46
60	11.58	4.46	5.18	11.03	1.94	5.43	10.83	1.94	5.53

Table 5.9 Comparison of Pseudo-First-Order/ Pseudo-Second-Order Kinetic Constants

Conc. of Metal Ions (mg/L)	$q_{exp.}$ (mg/g)	Pseudo-First-order kinetics				Pseudo-Second-order kinetics			
		$q_{cal.}$ (mg/g)	$k_1 \times 10^{-3}$ (min^{-1})	R^2	SSE	$q_{cal.}$ (mg/g)	$k_2 \times 10^{-3}$ (g/ mg min)	R^2	SSE
Pb(II)									
50	7.80	4.33	0.69	0.9097	2.00	6.32	4.63	0.9931	0.36
100	13.40	7.12	0.92	**0.9410**	**6.57**	11.57	3.05	**0.9902**	**0.55**
150	10.48	6.50	0.91	0.9272	2.64	9.10	7.40	0.9965	0.31
200	13.02	5.37	0.53	0.9182	9.80	12.64	4.41	0.9990	0.02
250	12.80	5.92	0.11	0.9044	7.88	11.71	3.17	0.9933	0.19
Cd(II)									
50	7.19	10.01	0.23	0.8551	1.32	6.15	5.48	0.9895	0.18
100	12.82	8.86	0.76	**0.9243**	**2.61**	10.61	3.07	**0.9970**	**0.81**
150	10.17	9.43	0.23	0.8337	1.01	9.29	3.94	0.9960	0.12
200	11.96	5.05	0.46	0.8854	7.95	10.20	2.63	0.9915	0.51
250	12.38	6.28	0.42	0.8504	6.20	11.34	3.11	0.9946	0.18
Ni(II)									
50	6.55	4.07	0.23	0.8604	1.02	5.80	8.93	0.995	0.09
100	12.41	5.63	0.47	**0.9418**	**7.66**	11.61	3.61	**0.9951**	**0.10**
150	9.12	6.54	0.26	0.8405	1.10	7.63	3.82	0.9861	0.37
200	9.14	10.96	0.28	0.8345	1.29	8.02	6.38	0.9963	0.20
250	11.20	10.03	0.21	0.8117	1.22	10.04	5.44	0.9915	0.22

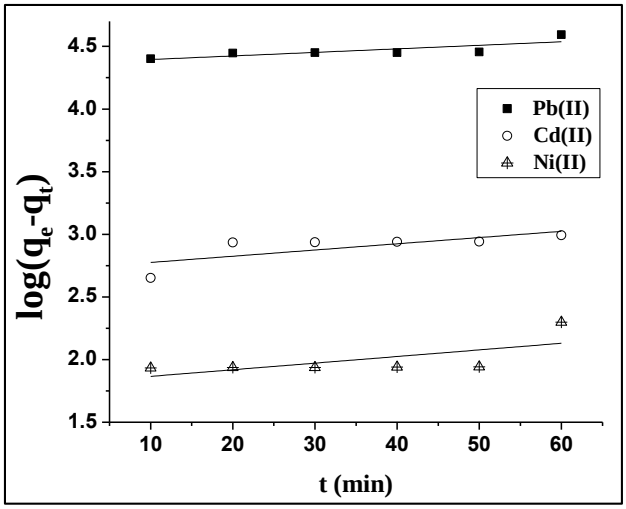

Figure 5.26 Pseudo-First-Order Kinetics

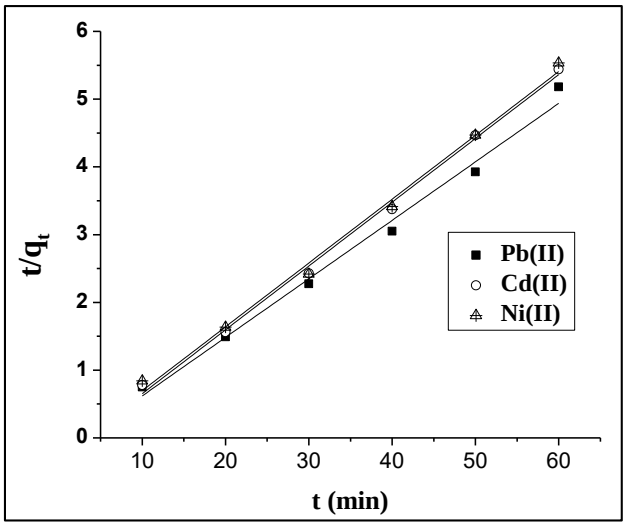

Figure 5.27 Pseudo-Second-Order Kinetics

5.7.2 Elovich Model

Figure 5.28 represents the Elovich plot and the kinetic constants α, β (Table 5.10) calculated from the graph shows a trend of better inclined 'β' values (extent of surface coverage), thence an unavailability of active sites for the sorbent adhesion at higher concentrations is obvious.

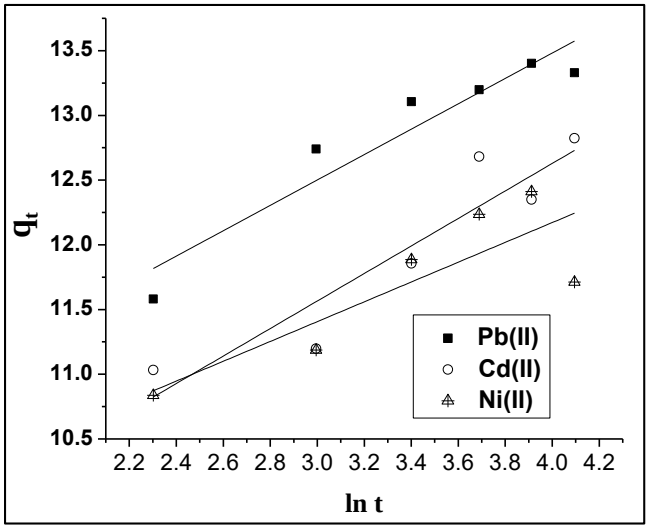

Figure 5.28 Elovich Model

Table 5.10 Elovich Constants

Conc. of Metal Ions (mg/L)	Pb(II)			Cd(II)			Ni(II)		
	α	β	R^2	α	β	R^2	α	β	R^2
50	0.68	4.88	0.8749	0.59	4.86	0.9458	0.35	5.01	0.7760
100	0.98	9.55	0.9059	1.06	8.37	0.9659	0.76	9.10	0.7019
150	0.52	7.93	0.7978	0.85	6.44	0.9098	0.75	6.13	0.8023
200	1.01	8.87	0.8871	1.36	6.25	0.9472	0.44	7.09	0.7003
250	0.98	8.67	0.9505	1.04	8.12	0.9661	0.66	8.41	0.8589

α: (mg/g min), β: (g/mg)

5.7.3 Intraparticle Diffusion Model

Weber and Morris intraparticle diffusion plots (Figure 5.29) reveals two distinct portions[145] i.e; initial rapid adsorption followed by slow diffusion. The intraparticle rate constant (K_i) and boundary layer thickness (C) values (Table 5.11) figured from the plot, registered a steady increase with initial metal concentrations[149]. This may be because of a decline in mass transfer resistance onto the surface of TTIH.

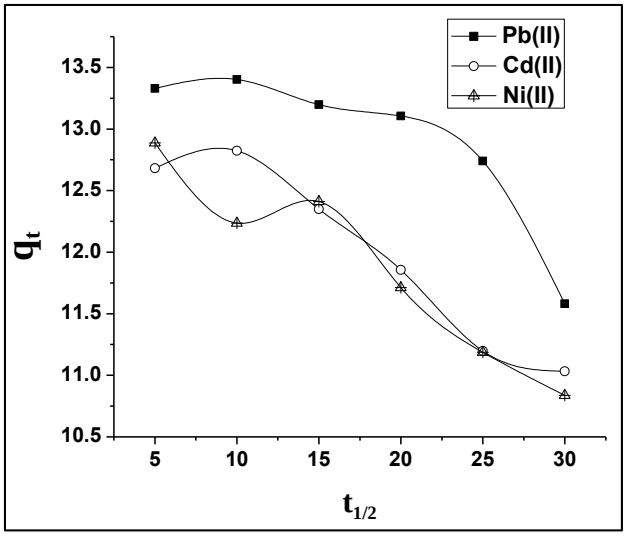

Figure 5.29 Intraparticle Diffusion Model

Table 5.11 Intraparticle Diffusion Constants

Conc. of Metal Ions (mg/L)	Pb(II)		Cd(II)		Ni(II)	
	K_i (mg/g $min^{1/2}$)	C	K_i (mg/g $min^{1/2}$)	C	K_i (mg/g $min^{1/2}$)	C
50	0.04	8.02	0.03	7.70	0.03	7.13
100	0.06	13.97	0.07	13.35	0.08	13.28
150	0.09	11.37	0.05	10.37	0.07	10.23
200	0.06	13.48	0.09	12.52	0.05	9.73
250	0.05	13.14	0.06	12.89	0.05	11.92

5.8 Adsorption Dynamics

The thermodynamic parameters ΔH^0, ΔS^0 calculated from the slopes and intercepts of Vant Hoff's plot (Figure 5.30) are shown in table 5.12. The positiveness of ΔH^0 and ΔS^0 values suggest the endothermic nature and extended mobility at the solid-solution interface during adsorption process[108]. The negative ΔG^0 values determine the spontaneous nature of sorption[141] for Pb(II), Cd(II) and Ni(II) systems.

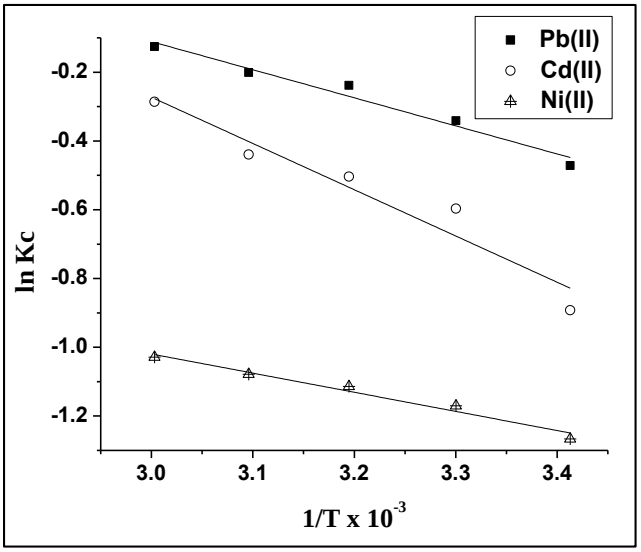

Figure 5.30 Vant Hoff's Plot

Table 5.12 Thermodynamic Constants

Temp. K	Pb(II)			Cd(II)			Ni(II)		
	ΔG°x10^{-3} kJ/mol	ΔH° kJ/mol	ΔS° J/mol K	ΔG°x10^{-3} kJ/mol	ΔH° kJ/mol	ΔS° J/mol K	ΔG°x10^{-3} kJ/mol	ΔH° kJ/mol	ΔS° J/mol K
293	-1.14			-2.17			-3.08		
303	-0.85			-1.35			-2.94		
313	-0.62	6.78	19.44	-1.31	5.18	11.29	-2.89	3.62	5.40
323	-0.54			-1.18			-2.89		
333	-0.43			-0.79			-3.01		

5.9 Effect of TTIH on Industrial Effluents

The influence of different doses of TTIH upon the collected effluents and prepared synthetic solutions are shown in figure 5.31. Heightening of curves are maximum at a dose of 750 mg representing it as the required dosage for enhanced trapping of the metal ions from respective dilutions (referred in 3.12).

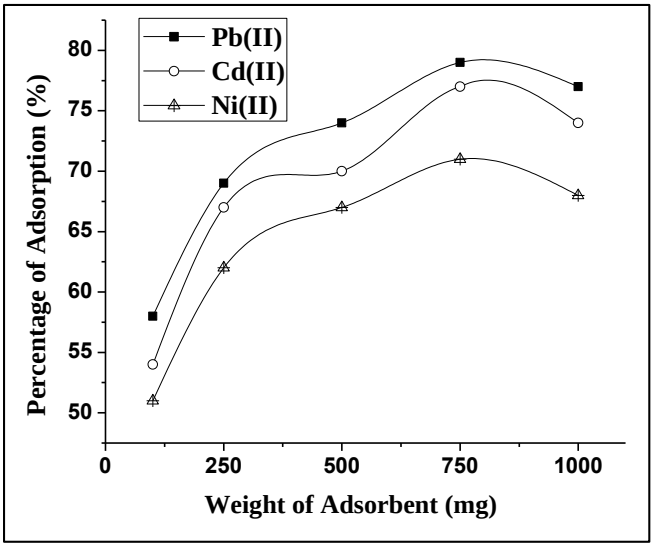

Figure 5.31 Effect of TTIH on Effluent/ Synthetic Solutions